Supplementary Information for the Paper Entitled:

Selective Adsorption of Fluorinated Super Greenhouse Gases within a Metal–Organic Framework with Dynamic Corrugated Ultramicropores

Bevan S. Whitehead, William W. Brennessel, Shane S. Michtavy, Hope A. Silva, Jaehwan Kim,
Phillip J. Milner, Marc D. Porosoff, and Brandon R. Barnett*

Table of Contents

1. General Considerations

Unless otherwise stated, all reagents and solvents were purchased from commercial sources and used as received. The metal–organic framework Zn(fba) was synthesized according to a published procedure.[1] The metal-organic frameworks Ni(3-ain)$_2$ and Ni(ina)$_2$ were synthesized according to a published procedure.[2] Activated charcoal used in breakthrough and sorption isotherm measurements was purchased from Fisher Scientific (catalog number AA1092622) and activated at 200 ºC under flowing N_2 (breakthrough) or ultrahigh vacuum (sorption).

Synthesis of Zn(fba). The following procedure was adapted from the literature.[1] A mixture of zinc acetate dihydrate with 4,4′-(hexafluoroisopropylidene) bis(benzoic acid) was heated in water at 170 °C for 2 days in a sealed bomb flask. The bomb flask was cooled to room temperature over a 24-hour period, then the white crystalline product was filtered using a coarse fritted funnel and washed three times with water and three times with acetone for 12 h each. The white crystalline product was dried at 60 °C on the Schlenk line to remove any remaining solvents and then transferred to a pre-weighed glass sorption tube capped with a check seal. The material was then fully activated by heating *in vacuo* (< 4 µbar) on a Micromeritics SmartVac at 110 ˚C for 24 hours.

2. Details of Gas Sorption Isotherm Measurements.

Adsorption isotherm measurements were performed on a Micromeritics 3Flex physisorption analyzer. Gas purities for all adsorbates (except for CHF_3) were ultrahigh purity or greater (at least 99.99% purity). Sieved MOF samples were prepared by pressing the material into a pellet, and then passing it through two different mesh sieves with openings of 0.25 mm and 0.50 mm, respectively. The fraction that passed through the 0.50 mm sieve, but not through the 0.25 mm sieve, was collected and used for isotherm measurements. For all adsorbates except for H_2O, an equilibration interval of 180 s was employed.

For water sorption measurements, ultrapure water (18.2 MΩ) from a Thermo Scientific Barnstead Nanopure system was transferred into the vapor source container for the Micromeritics 3Flex physisorption analyzer. Using a liquid nitrogen filled dewar and the vacuum on the 3Flex, the water was degassed five times via freeze-pump-thaw cycles to remove dissolved gases. Once degassed, vapor dosing experiments were started using an equilibration interval of 45 seconds and an analysis temperature of 298 K. For the experiment, the vapor dosing vessel was heated to 35 °C using a heating mantle.

Isotherm Fitting, Differential Enthalpies of Adsorption, and IAST Calculations. Single-component adsorption isotherms were fit individually using a dual-site Langmuir Freundlich equation, given by:

$$n = \frac{q_{(sat,a)} b_a\, p^{v_a}}{1+b_a\, p^{v_a}} + \frac{q_{(sat,b)} b_b\, p^{v_b}}{1+b_b\, p^{v_b}} \tag{1}$$

where n is the amount adsorbed in mmol/g, q_{sat} is the amount adsorbed when saturated with the gas in mmol/g, b is the Langmuir parameter in bar^{-1}, P is the gas pressure in bar, v is the dimensionless Freundlich parameter, and subscripts a and b correspond to two different site identities. These parameters were determined using a least-squares method and are given in Tables S2–4. The differential enthalpies of adsorption as a function of gas loading were extracted from the fits of single-component isotherms at 288, 298 and 308 K. The isotherm fits were numerically inverted and solved as $P(n)$. The enthalpy h can then be determined at constant loadings using the Clausius–Clapeyron relationship:

$$h = -R\frac{\left(d(\ln P)\right)}{\left(d\left(\frac{1}{T}\right)\right)} \quad (2)$$

where R is the ideal gas constant, P is the pressure at a given loading, and T is the temperature at which the isotherm data were collected.

Ideal Adsorbed Solution Theory (IAST) was used to determine adsorbent selectivity from single-component gas adsorption isotherms.[3] This approach involves numerically solving for the spreading pressure and subsequently determining the composition of the adsorbed phase at a given gas phase composition. The selectivity S for adsorption of a from a two-component mixture comprised of a and b is then given by:

$$S = \frac{x_a/x_b}{y_a/y_b} \quad (3)$$

where x is the mole fraction in the adsorbed phase, y is the mole fraction in the gas phase, and the subscripts a and b refer to the mixture components.

BET Analysis of Zn(fba).

The general form of the BET equation is,

$$\frac{x}{v(1-x)} = \frac{1}{v_m c} + \frac{(c-1)}{v_m c} \cdot x \quad (4)$$

Where, v is the adsorption value at the relative pressure, x (=P/P_0), which is the equilibrium pressure normalized by the saturation vapor pressure (P_0) of the adsorbate at the same temperature, v_m is the adsorption value corresponding to the monolayer, and c = exp (E_1-E_L)/RT.

$$v(P_0 - P) = \frac{P_0 V_m c x}{1+x(c+1)} \quad (5)$$

If we differentiate equation (5) with respect to x, we obtain,

$$\frac{d\left(v(P_0-P)\right)}{dx} = \frac{d}{dx}\left(\frac{P_0 v_m c x}{1+x(c+1)}\right) \quad (6)$$

$$= \frac{P_0 v_m c}{\left(1+x(c-1)\right)^2}$$

Here, P_0 and v_m are positive values, and c should be a positive value to satisfy the second consistency criterion. Thus, the right-hand side of equation (6) should be positive if the BET plot satisfies the second consistency criterion ($c > 0$). From this, we can conclude that the left-hand side of equation (3) should be also positive. This means that the term v(P_0 – P) should continuously increase with increasing x. This satisfies the first consistency criterion for BET surface area calculations. Using the 87 K Argon isothermal data between the range of $0.005 < x < 0.01$, chosen to satisfy the consistency criterion and the ultra-microporosity of the two different types of pores, a linear fit can be calculated with the equation y=mx+b. This fit can then be used to calculate the c and v_m values using equation (6). These values could then be plugged into equation (7):

$$BET\ Surface\ Area = v_m \sigma_0 N_{av}\ (7)$$

Where σ_0 is equal to the cross-sectional area of argon at liquid density (14.3Å) and N_{av} is Avogadro's number.

Table S1. Previous reports of CF_4/N_2 selectivity in solid-state framework materials. All selectivity values are for a 10:90 mixture unless otherwise specified.

Material	10:90 CF_4:N_2 IAST selectivities (Unless otherwise noted)	Reference	Notes
Ni(3-ain)$_2$	46.3	2	
Ni(ina)$_2$	34.7	2	
Zn(fba)	29.0	This Work	
$Ni_3(HCOO)_6$	25	4	
Ni(ADC)(DABCO)$_{0.5}$	23	5	
C-PVDC-600	18.6	6	
PDC-2-700	18	7	
Al-Fum	16.5	8	
ACK1	15.2	9	
C-PVDC-800	13.9	6	
C-PVDC-900	13.6	6	
C-PVDC-700	13.2	6	
PET-K(2)700	12.6	10	
PC450-K2	12.5	11	
$Co_3(HCOO)_6$	12	4	
$Mn_3(HCOO)_6$	12	4	
TiC-CDC800H	11.6	12	
α-SiC-CDC1100	10	13	
Zeolite 5A	9.49	13	
MOF-303	8.4	8	
SBMOF-1	7.3	14	
POPTrA-8F	6.18	15	1:99 CF_4:N_2
Ni(pba)$_2$	6.04	2	
POPTrB-4F	5.71	15	1:99 CF_4:N_2
POPTrA-4F	5.66	16	1:99 CF_4:N_2
POPTrB-8F	5.34	16	1:99 CF_4:N_2
MIL-160	4.8	8	
Zeolite 13X	3.17	17	
Cu(peba)	2.25	2	
Darco Activated Carbon	2.25	17	
Ni-MOF-74	2.19	2	
Silica Gel	1.11	18	
APA Activated Carbon	1.09	12	
F400 Activated Carbon	0.95	12	

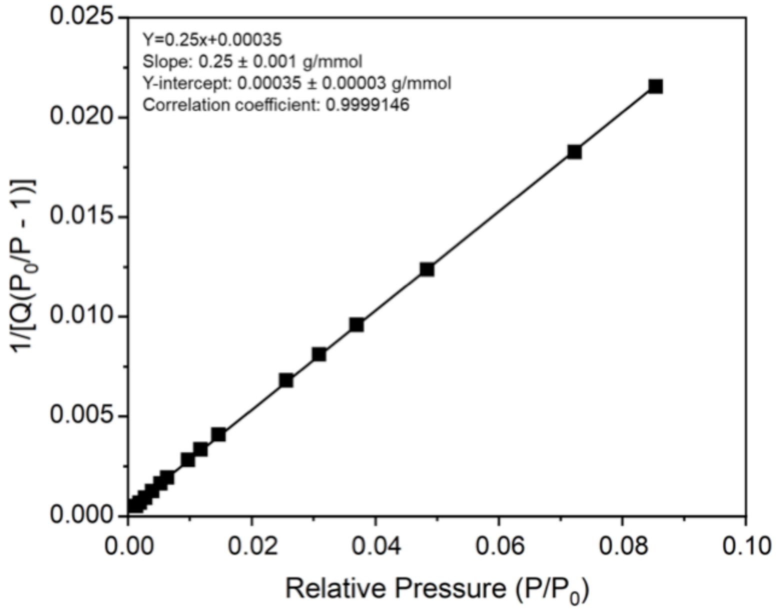

Figure S1. BET fitting of Zn(fba) within the range of $0.005 < x < 0.01$. Using the BET equation, $c = 720$ and $v_m = 4.01$ mmol/g were calculated. Using equation (7), Area=$v_m \sigma_0 N_{av}$, a BET surface area of 345 ± 1.2 m²/g was calculated.

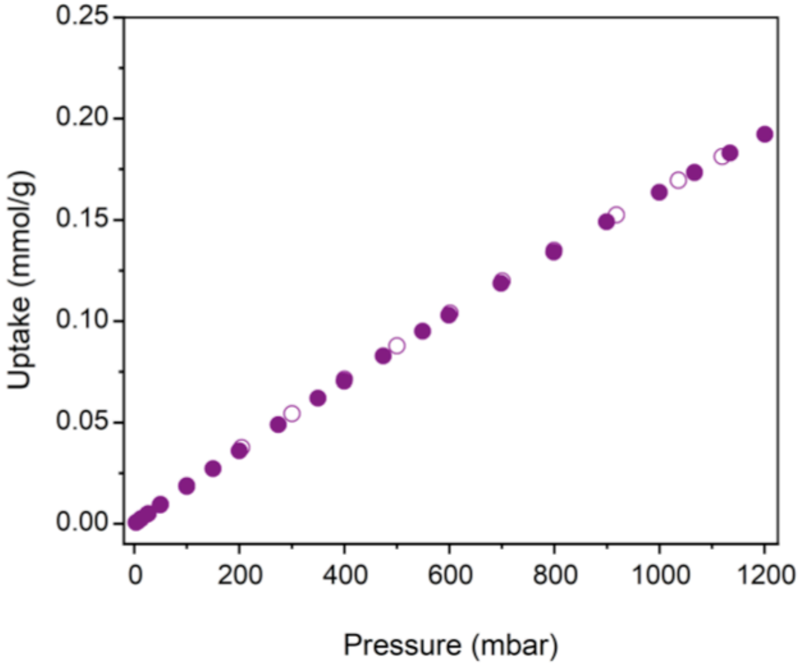

Figure S2. Argon sorption data for Zn(fba) at 298 K.

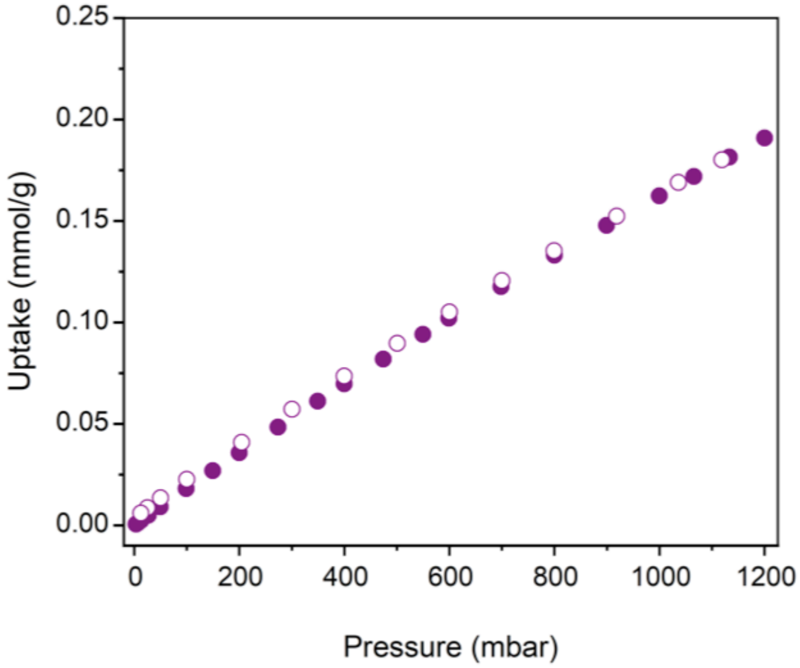

Figure S3. Oxygen sorption data for Zn(fba) at 298 K.

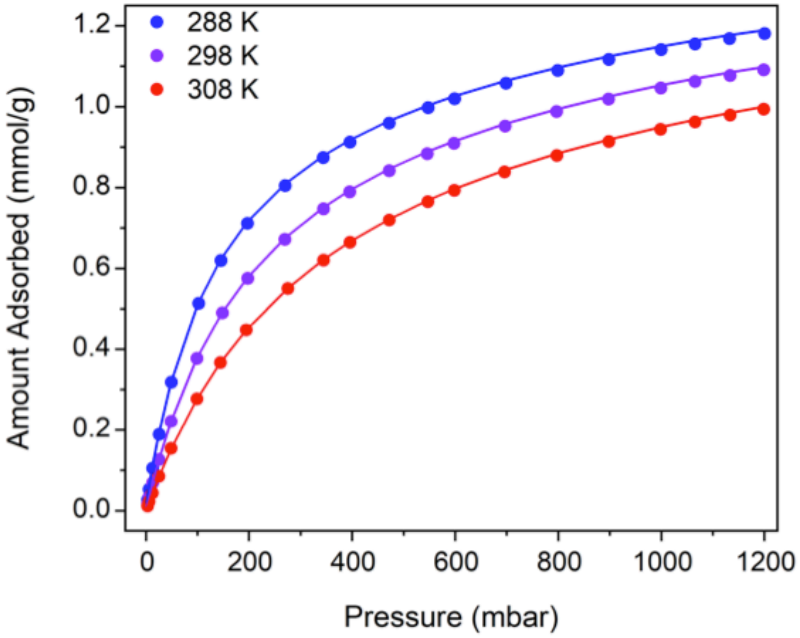

Figure S4. Single-component CF_4 adsorption isotherms (data points) and corresponding fits (solid lines) for Zn(fba) at 288, 298, and 308 K.

Table S2. Dual-site Langmuir-Freundlich fit parameters for all Zn(fba) tetrafluoromethane isotherms.

Tetrafluoromethane			
$\boldsymbol{T}$ **(K)**	288	298	308
$\boldsymbol{q_{\text{sat,a}}}$ **(mmol/g)**	1.13	1.17	0.37
$\boldsymbol{b_{\text{a}}}$ **(bar^{-1})**	7.90	4.80	0.31
$\boldsymbol{v_{\text{a}}}$	1.01	1.00	1.11
$\boldsymbol{q_{\text{sat,b}}}$ **(mmol/g)**	0.36	0.26	1.12
$\boldsymbol{b_{\text{b}}}$ **(bar^{-1})**	0.61	0.46	3.19
$\boldsymbol{v_{\text{b}}}$	1.29	1.51	1.00

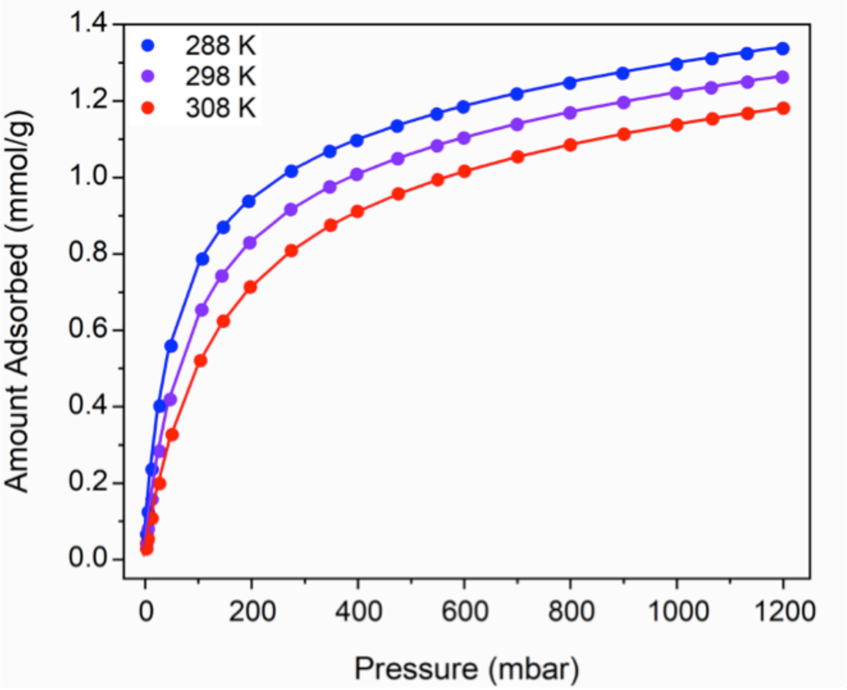

Figure S5. Single-component CHF_3 isotherms and corresponding fits for Zn(fba) at 288, 298, and 308 K.

Table S3. Dual-site Langmuir-Freundlich fit parameters for all Zn(fba) trifluoromethane isotherms.

Trifluoromethane			
T (K)	288	298	308
$q_{\mathrm{sat,a}}$ (mmol/g)	0.66	0.67	1.12
b_{a} (bar^{-1})	0.57	0.42	8.17
v_{a}	1.13	1.12	1.01
$q_{\mathrm{sat,b}}$ (mmol/g)	1.11	1.10	0.51
b_{b} (bar^{-1})	20.67	13.00	0.37
v_{b}	1.01	1.01	1.21

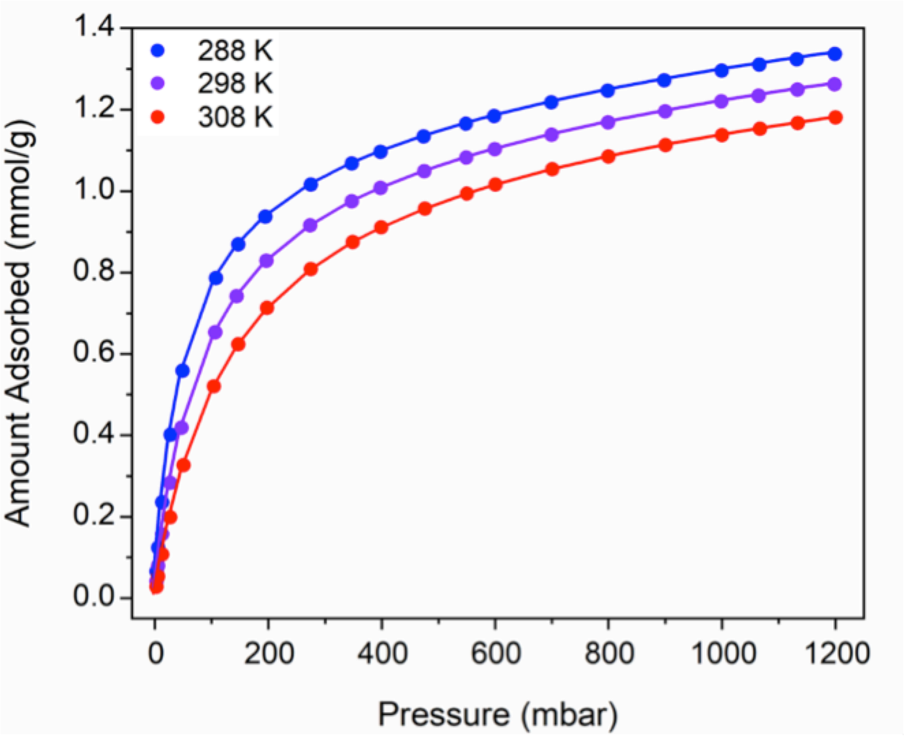

Figure S6. Single-component methane isotherms and corresponding fits for Zn(fba) at 288, 298, and 308 K.

Table S4. Dual-site Langmuir-Freundlich fit parameters for all Zn(fba) methane isotherms.

Methane			
***T* (K)**	288	298	308
$q_{\mathrm{sat,a}}$ (mmol/g)	0.72	0.82	0.39
b_{a} (bar^{-1})	2.14	1.35	0.39
v_{a}	1.04	1.01	0.93
$q_{\mathrm{sat,b}}$ (mmol/g)	0.60	0.43	0.88
b_{b} (bar^{-1})	0.65	0.60	0.94
v_{b}	0.89	0.98	1.01

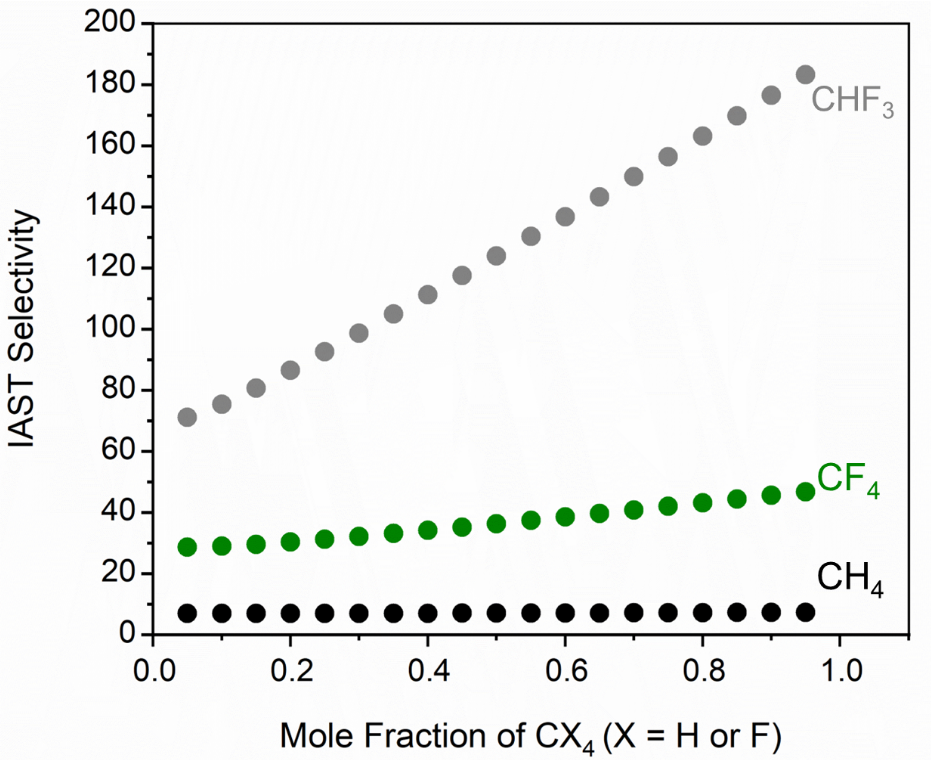

Figure S7. Two-component CX_4/N_2 IAST selectivity as a function of C_1 mole fraction. Calculations were performed for $T = 298$ K and $P_{\mathrm{tot}} = 1$ bar.

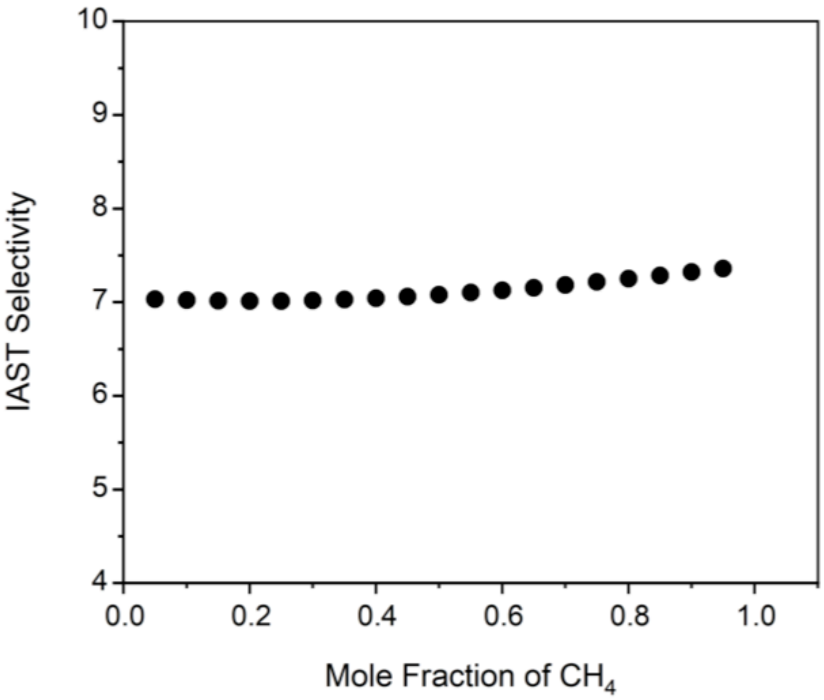

Figure S8. Two-component CH_4/N_2 selectivity as a function of CH_4 mole fraction. Note this is the same data shown in Figure S7.

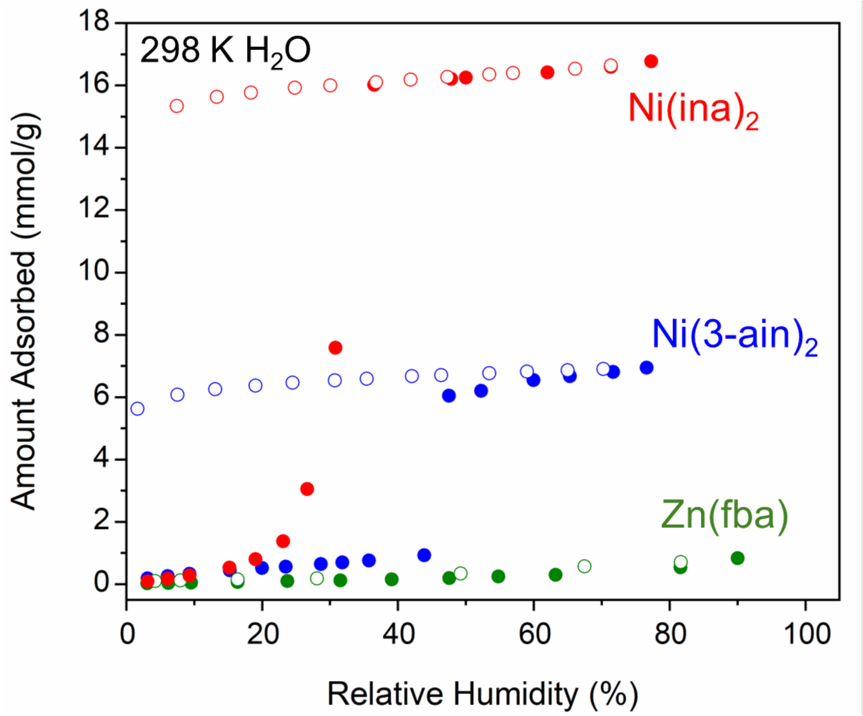

Figure S9. Water sorption isotherms at 298 K for Zn(fba), Ni(ina)$_2$, and Ni(3-ain)$_2$.

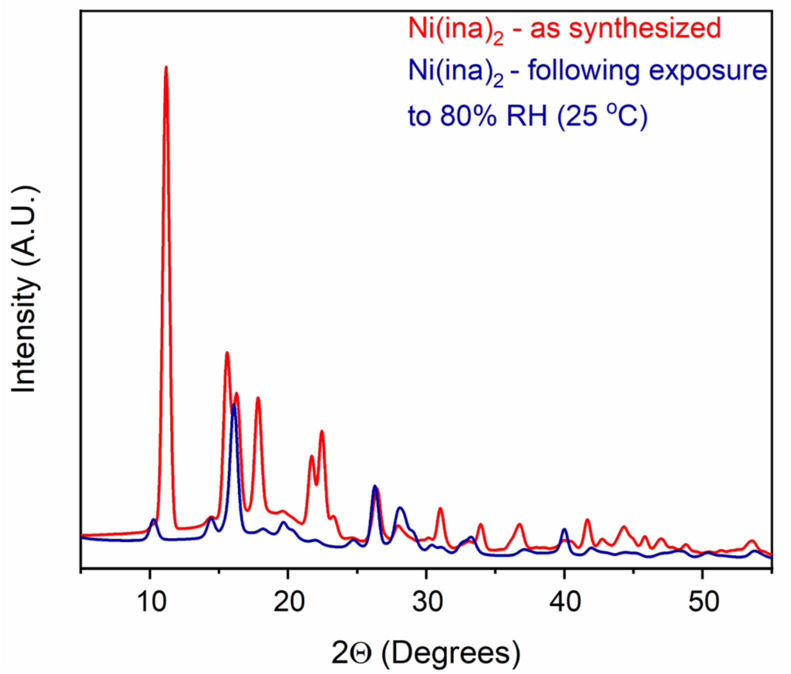

Figure S10. Powder X-ray diffraction data of Ni(ina)$_2$, showing both the as-synthesized material (red) and following collection of the water isotherm data shown in Figure S9. λ = 1.5406 Å

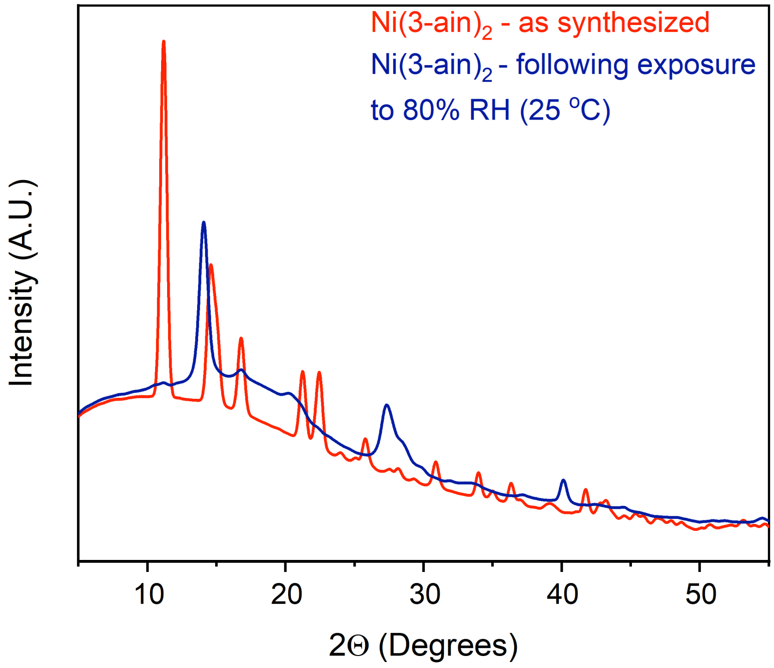

Figure S11. Powder X-ray diffraction data of Ni(3-ain)$_2$, showing both the as-synthesized material (red) and following collection of the water isotherm data shown in Figure S9. λ = 1.5406 Å.

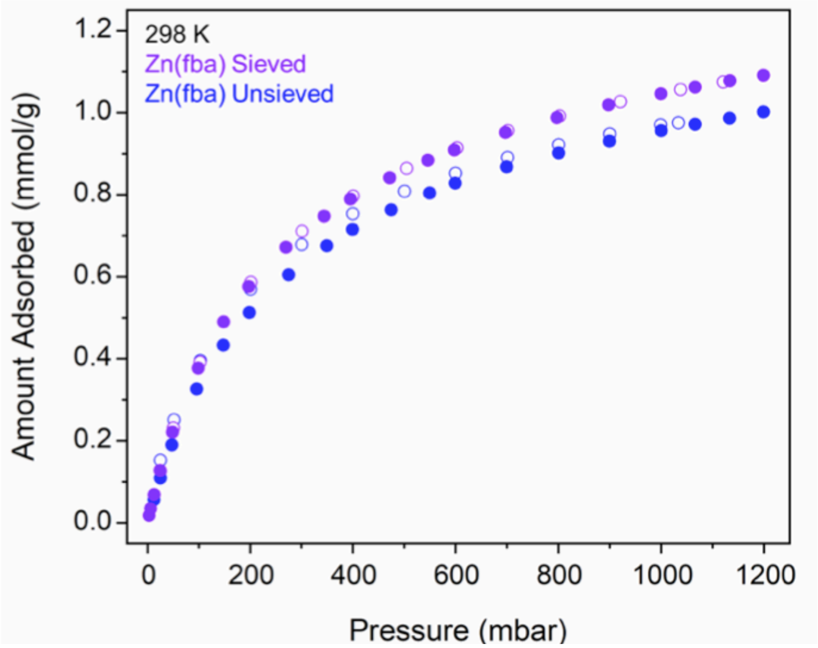

Figure S12. Tetrafluoromethane adsorption isotherms for unsieved (i.e. as synthesized) and sieved Zn(fba) samples at 298 K. Closed and open circles correspond to adsorption and desorption sweeps, respectively.

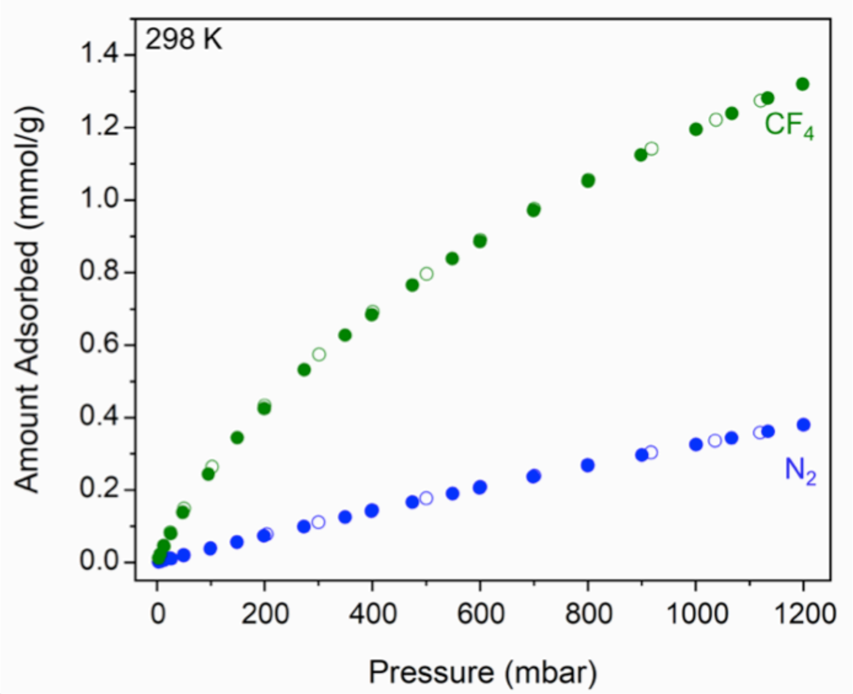

Figure S13. Tetrafluoromethane and nitrogen isotherms at 298 K tetrafluoromethane and N_2 isotherms of activated charcoal. Using IAST, the selectivity of the material for CF_4 vs. N_2 (5:95 ratio at 1 bar total pressure) was calculated to be 7.9.

3. Solid-State ^{19}F NMR Measurements

A sample of Zn(fba) that had been dosed with 1 bar of CF_4 in a Micromeritics sorption tube was brought into a N_2-filled glovebox and packed within a 35 µL rotor. The rotor was transferred to a 20 mL scintillation vial, which was then threaded with Teflon tape and taped before being brought out of the glovebox and transported to the NMR spectrometer for immediate analysis.

Magic angle spinning (MAS) solid-state NMR measurements were carried out using a Phoenix NMR HX NB Probe (3.2 mm) located within a Varian INOVA 500 MHz spectrometer. All MAS SSNMR experiments were carried out using samples packed within 35 µL rotors at a spinning speed of 20 kHz. ^{19}F chemical shifts were referenced to $CFCl_3$ at 0 ppm using Teflon as a secondary reference (−123.2 ppm).

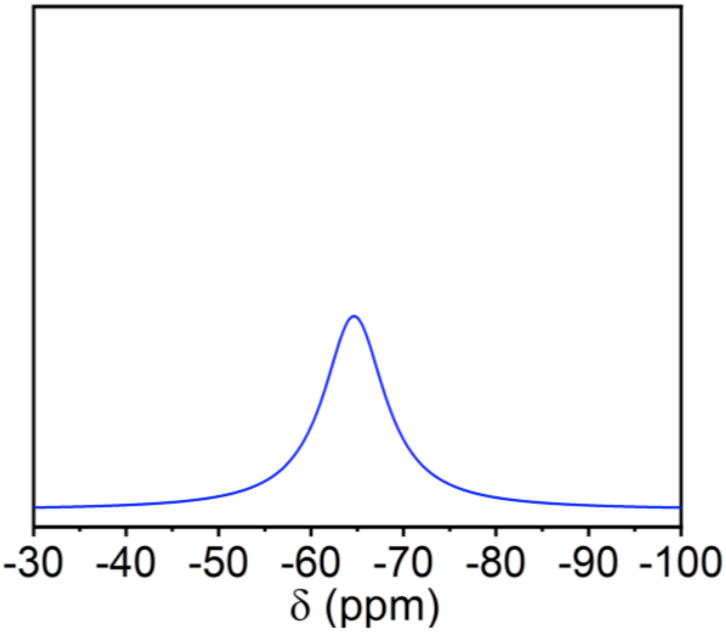

Figure S14. ^{19}F Magic Angle Spinning solid-state NMR of activated Zn(fba).

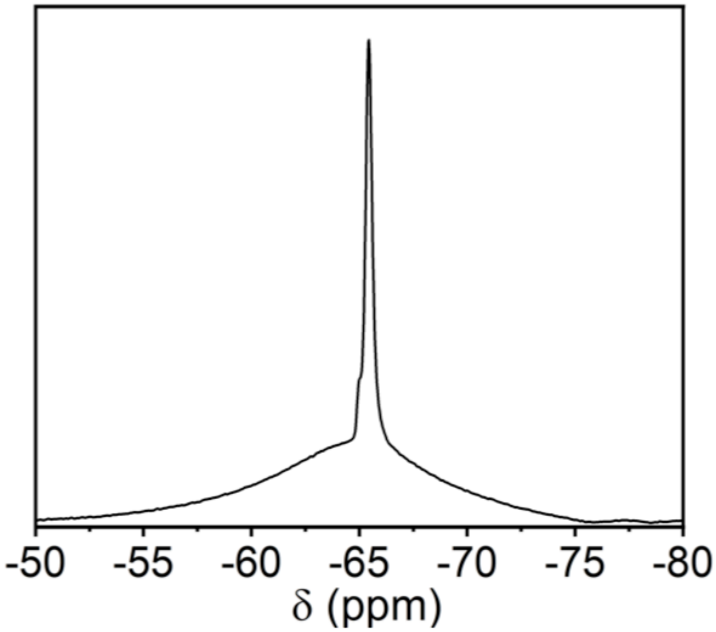

Figure S15. ^{19}F Magic Angle Spinning solid-state NMR spectrum of CF_4-dosed Zn(fba).

4. Thermogravimetric Analysis

Thermogravimetric decomposition measurements were performed on a TA instruments TGA55 under an atmosphere of N_2 gas with a ramp rate of 0.5 °C/min from 25 °C to 300 °C and then at 10 °C/min from 300 °C to 600 °C. A Zn(fba) sample was dosed with tetrafluoromethane and allowed to equilibrate for 12 hours. The material was then transferred to a pre-weighed disposable aluminium pan, which was loaded onto a platinum carrier pan. This was loaded into the instrument.

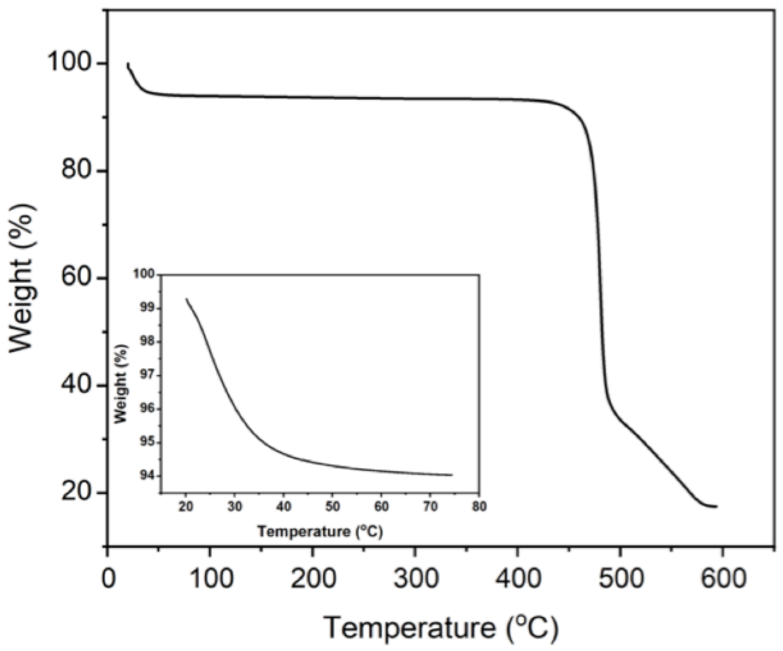

Figure S16. TGA of Zn(fba) dosed with 1 bar of tetrafluoromethane and allowed to equilibrate for 12 hours. The material was transferred in air into a TGA pan. The temperature was ramped at the rate of 0.5 °C/min from 25 °C to 300 °C, and then at 10 °C/min from 300 °C to 600 °C. The initial loss of mass corresponds to desorption of tetrafluoromethane.

5. Single Crystal X-ray Diffraction Measurements.

An acetone-solvated crystal of Zn(fba) was mounted into a 0.3 mm glass capillary tube, which was connected to a capillary-dosing assembly attached to a port on a Micromeritics 3 Flex gas sorption analyzer, see Figure S17. The sample was evacuated under reduced pressure at 110 °C for 24 h to remove all solvent molecules within the crystal. The capillary was then dosed with tetrafluoromethane or methane (1 bar) and then flame-sealed closed using a methane/oxygen torch. The capillary-sealed crystals were mounted on a Rigaku XtaLAB Synergy-S Dualflex diffractometer equipped with a HyPix-6000HE HPC area detector for data collection. A preliminary set of cell constants and an orientation matrix were calculated from a small sampling of reflections.[19] A short pre-experiment was run, from which an optimal data collection strategy was determined. The full data collection was carried out using a PhotonJet (Cu) X-ray source at a detector-to-sample distance of 34.0 mm. Series of frames were collected in 0.50º steps in ω at different 2θ, κ, and φ settings. After the intensity data were scaled and corrected for absorption, the final cell constants were calculated from the *xyz* centroids of the strong reflections from the actual data collection after integration.[20]

The structure was solved using *SHELXT*[20] and refined using *SHELXL*.[21] The space group $P6_222$ was determined based on systematic absences and intensity statistics. Most or all non-hydrogen atoms were assigned from the solution. Full-matrix least squares / difference Fourier cycles were performed which located any remaining non-hydrogen atoms. All non-hydrogen atoms were refined with anisotropic displacement parameters. All hydrogen atoms were placed in ideal positions and refined as riding atoms with relative isotropic displacement parameters. The final full matrix least squares refinement against F^2 was run to convergence. Structure manipulation was performed using *Olex2*.[22] The same parameters and methods for integration, scaling, and data corrections (*e.g.* absorption) were applied to each experiment, although the scan scenarios and scan times were slightly different for each. The same solution was used to start each refinement, and each refinement was performed identically for consistency.

CCDC Deposition. The .cif files associated with each crystallographic determination have been deposited to the Cambridge Crystallographic Data Centre (CCDC numbers 2321191–2321195).

Figure S17. Custom-built capillary dosing set up shown on the countertop and attached to the Micromeritics Smart VacPrep.

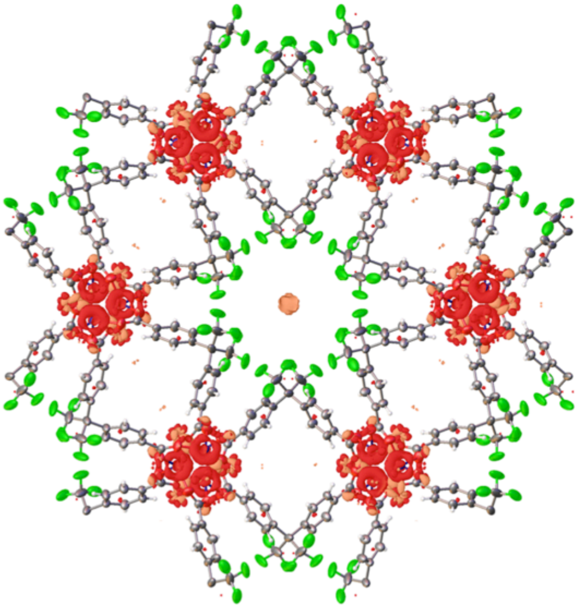

Figure S18. Residual electron density within an activated crystal of Zn(fba) as determined by X-ray diffraction at 298 K. Orange and red regions correspond to positive and negative electron density, respectively. Density isosurface values are set at 0.33 e/Å^3. The small amount of positive density at the center of the fluorinated channel (which corresponds to a crystallographic special position) is consistently seen in the activated material and is tentatively suggested to be a crystallographic artifact.

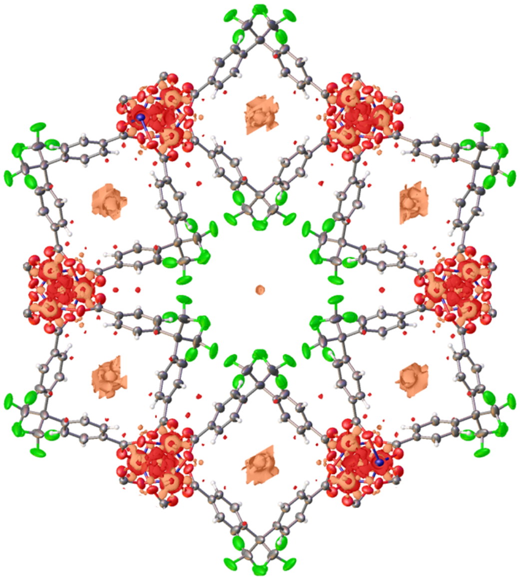

Figure S19. Residual electron density within an activated crystal of Zn(fba) dosed with 1 atmosphere of Methane as determined by X-ray diffraction at 250 K. Orange and red regions correspond to positive and negative electron density, respectively. Density isosurface values are set at 0.43 e/Å^3.

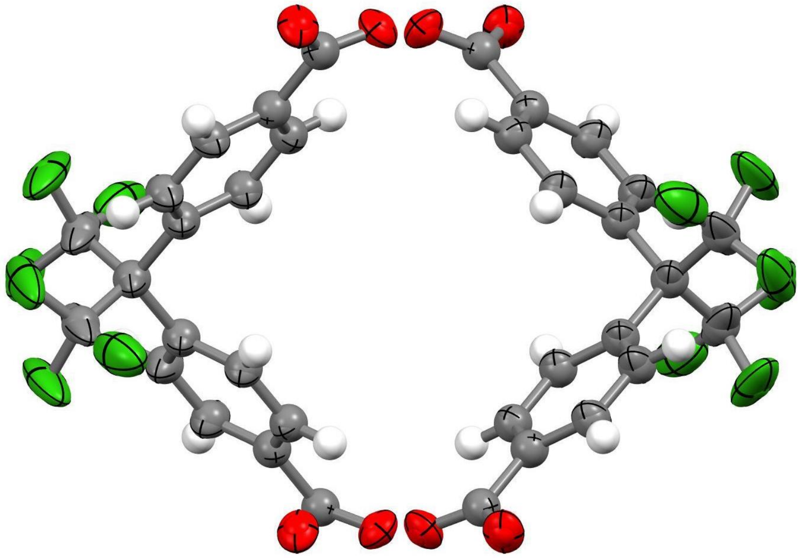

Figure S20. Overlaid structures of activated and CF_4-dosed (1 bar) structures of Zn(fba) at 298 K, showing two adjacent fba^{2-} linkers that define a singular pore window (center). For differentiation, the activated structure is depicted using a ball and stick style, while the dosed structure is depicted with thermal ellipsoids (50% probability).

Table S5. Crystal data and structure refinement for activated Zn(fba) at 298 K.

Identification code	brbbsw97	
Empirical formula	C17 H8 F6 O4 Zn	
Formula weight	455.60	
Temperature	298.00(10) K	
Wavelength	1.54184 Å	
Crystal system	hexagonal	
Space group	P 62 2 2	
Unit cell dimensions	*a* = 21.2076(5) Å	α = 90°
	b = 21.2076(5) Å	β = 90°
	c = 7.7012(2) Å	γ = 120°
Volume	2999.66(16) Å^3	
Z	6	
Density (calculated)	1.513 Mg/m^3	
Absorption coefficient	2.406 mm^{-1}	
F(000)	1356	
Crystal color, morphology	colourless, needle	
Crystal size	0.169 x 0.04 x 0.018 mm^3	
Theta range for data collection	2.406 to 80.370°	
Index ranges	$-27 \leq h \leq 25$, $-26 \leq k \leq 27$, $-9 \leq l \leq 6$	
Reflections collected	17349	
Independent reflections	2182 [*R*(int) = 0.1166]	
Observed reflections	1716	
Completeness to theta = 67.684°	100.0%	
Absorption correction	Multi-scan	
Max. and min. transmission	1.00000 and 0.02411	
Refinement method	Full-matrix least-squares on F^2	
Data / restraints / parameters	2182 / 0 / 128	
Goodness-of-fit on F^2	1.081	
Final *R* indices [I>2sigma(I)]	*R*1 = 0.0383, *wR*2 = 0.0775	
R indices (all data)	*R*1 = 0.0627, *wR*2 = 0.0887	
Absolute structure parameter	0.01(3)	
Extinction coefficient	n/a	
Largest diff. peak and hole	0.297 and -0.495 e.Å^{-3}	

Table S6. Crystal data and structure refinement for CF_4-dosed Zn(fba) at 298 K.

Identification code	brbbsw99	
Empirical formula	C17 H8 F6 O4 Zn	
Formula weight	455.60	
Temperature	298.00(10) K	
Wavelength	1.54184 Å	
Crystal system	hexagonal	
Space group	P 62 2 2	
Unit cell dimensions	a = 21.2035(5) Å	α = 90°
	b = 21.2035(5) Å	β = 90°
	c = 7.6959(2) Å	γ = 120°
Volume	2996.44(16) Å^3	
Z	6	
Density (calculated)	1.515 Mg/m^3	
Absorption coefficient	2.408 mm^{-1}	
F(000)	1356	
Crystal color, morphology	colourless, needle	
Crystal size	0.169 x 0.04 x 0.018 mm^3	
Theta range for data collection	2.406 to 80.324°	
Index ranges	$-23 \leq h \leq 26$, $-27 \leq k \leq 26$, $-9 \leq l \leq 4$	
Reflections collected	12102	
Independent reflections	2176 [R(int) = 0.0921]	
Observed reflections	1732	
Completeness to theta = 67.684°	100.0%	
Absorption correction	Multi-scan	
Max. and min. transmission	1.00000 and 0.03706	
Refinement method	Full-matrix least-squares on F^2	
Data / restraints / parameters	2176 / 0 / 128	
Goodness-of-fit on F^2	1.024	
Final R indices [I>2sigma(I)]	R1 = 0.0399, wR2 = 0.0942	
R indices (all data)	R1 = 0.0598, wR2 = 0.1032	
Absolute structure parameter	0.00(3)	
Extinction coefficient	n/a	
Largest diff. peak and hole	0.396 and -0.563 e.Å^{-3}	

Table S7. Crystal data and structure refinement for CF_4-dosed Zn(fba) at 273 K.

Identification code	brbbsw99_273	
Empirical formula	C17 H8 F6 O4 Zn	
Formula weight	455.60	
Temperature	272.99(10) K	
Wavelength	1.54184 Å	
Crystal system	hexagonal	
Space group	P 62 2 2	
Unit cell dimensions	a = 21.2008(6) Å	α = 90°
	b = 21.2008(6) Å	β = 90°
	c = 7.6911(2) Å	γ = 120°
Volume	2993.80(19) $Å^3$	
Z	6	
Density (calculated)	1.516 Mg/m^3	
Absorption coefficient	2.410 mm^{-1}	
F(000)	1356	
Crystal color, morphology	colourless, needle	
Crystal size	0.169 x 0.04 x 0.018 mm^3	
Theta range for data collection	2.406 to 80.040°	
Index ranges	$-18 \le h \le 26$, $-26 \le k \le 16$, $-9 \le l \le 4$	
Reflections collected	10348	
Independent reflections	2168 [R(int) = 0.0535]	
Observed reflections	1755	
Completeness to theta = 67.684°	99.9%	
Absorption correction	Multi-scan	
Max. and min. transmission	1.00000 and 0.01203	
Refinement method	Full-matrix least-squares on F^2	
Data / restraints / parameters	2168 / 0 / 128	
Goodness-of-fit on F^2	1.055	
Final R indices [I>2sigma(I)]	$R1$ = 0.0344, $wR2$ = 0.0763	
R indices (all data)	$R1$ = 0.0519, $wR2$ = 0.0820	
Absolute structure parameter	0.02(2)	
Extinction coefficient	n/a	
Largest diff. peak and hole	0.244 and -0.178 e.$Å^{-3}$	

Table S8. Crystal data and structure refinement for CF_4-dosed Zn(fba) at 250 K.

Identification code	brbbsw99_250	
Empirical formula	C17 H8 F6 O4 Zn	
Formula weight	455.60	
Temperature	249.99(10) K	
Wavelength	1.54184 Å	
Crystal system	hexagonal	
Space group	P 62 2 2	
Unit cell dimensions	*a* = 21.2057(7) Å	α = 90°
	b = 21.2057(7) Å	β = 90°
	c = 7.6878(2) Å	γ = 120°
Volume	2993.9(2) $Å^3$	
Z	6	
Density (calculated)	1.516 Mg/m^3	
Absorption coefficient	2.410 mm^{-1}	
F(000)	1356	
Crystal color, morphology	colourless, needle	
Crystal size	0.169 x 0.04 x 0.018 mm^3	
Theta range for data collection	2.406 to 84.550°	
Index ranges	$-27 \le h \le 20$, $-26 \le k \le 26$, $-7 \le l \le 9$	
Reflections collected	13041	
Independent reflections	2183 [*R*(int) = 0.0661]	
Observed reflections	1715	
Completeness to theta = 67.684°	100.0%	
Absorption correction	Multi-scan	
Max. and min. transmission	1.00000 and 0.03086	
Refinement method	Full-matrix least-squares on F^2	
Data / restraints / parameters	2183 / 0 / 128	
Goodness-of-fit on F^2	1.017	
Final *R* indices [*I*>2sigma(*I*)]	*R*1 = 0.0368, *wR*2 = 0.0806	
R indices (all data)	*R*1 = 0.0592, *wR*2 = 0.0886	
Absolute structure parameter	-0.04(2)	
Extinction coefficient	n/a	
Largest diff. peak and hole	0.389 and -0.297 e.$Å^{-3}$	

Table S9. Crystal data and structure refinement for CH_4-dosed Zn(fba) at 250 K.

Identification code	brbbsw100	
Empirical formula	C17 H8 F6 O4 Zn	
Formula weight	455.60	
Temperature	250.00(10) K	
Wavelength	1.54184 Å	
Crystal system	hexagonal	
Space group	P 62 2 2	
Unit cell dimensions	*a* = 21.2065(6) Å	α = 90°
	b = 21.2065(6) Å	β = 90°
	c = 7.6905(3) Å	γ = 120°
Volume	2995.2(2) $Å^3$	
Z	6	
Density (calculated)	1.516 Mg/m^3	
Absorption coefficient	2.409 mm^{-1}	
F(000)	1356	
Crystal color, morphology	colourless, needle	
Crystal size	0.2 x 0.026 x 0.022 mm^3	
Theta range for data collection	2.406 to 81.434°	
Index ranges	$-19 \le h \le 26$, $-24 \le k \le 20$, $-9 \le l \le 7$	
Reflections collected	14225	
Independent reflections	2146 [*R*(int) = 0.1689]	
Observed reflections	1471	
Completeness to theta = 67.684°	99.5%	
Absorption correction	Multi-scan	
Max. and min. transmission	1.00000 and 0.04752	
Refinement method	Full-matrix least-squares on F^2	
Data / restraints / parameters	2146 / 0 / 128	
Goodness-of-fit on F^2	1.047	
Final *R* indices [*I*>2sigma(*I*)]	*R*1 = 0.0547, *wR*2 = 0.1368	
R indices (all data)	*R*1 = 0.1044, *wR*2 = 0.1783	
Absolute structure parameter	0.00(3)	
Extinction coefficient	n/a	
Largest diff. peak and hole	0.806 and -0.921 e.$Å^{-3}$	

6. Transient Adsorption Measurements.

Transient adsorption measurements were obtained on a Micromeritics 3Flex Physisorption Analyzer. The sorption sample tube containing Zn(fba) was outfitted with a glass rod so as to minimize the amount of interior free space. Following quantification of the free space volume using He gas at the analysis temperature and re-evacuation of the sample, the valve connecting the sample tube to the instrument manifold (which had been dosed with a known quantity of gas, typically 1.00 mmol/g) was automatically opened. This time point was defined as $t = 0$. The instrument software typically closed the aforementioned valve after approximately 15 seconds, at which point the MOF + gas was contained within a closed and undisturbed isothermal system. The DataMonitor software from Micromeritics was used to record the time-resolved quantities adsorbed at 0.5 s intervals.

Following a 1.00 mmol/g dose, adsorption of CH_4 at 298 K is approximately 90% complete by the time at which valve closing occurs (≈ 0.25 min). However, relatively little fractional uptake of CF_4 occurs within this time window. This conveniently allows for modeling to be carried out only on data points that follow this event, which obviates consideration of volume changes and gas flow while adsorption is occurring.

The difference in CF_4 pressure within the sample tube between $t = 0$ and equilibration (*i.e.* fractional uptake of unity) is approximately 10%. Employing the approximation that gas phase concentrations of CF_4 were invariant while adsorption occurs, fractional uptakes (defined here as q_t/q_e, where q_t and q_e are the quantities adsorbed at time t and at equilibrium, respectively) were plotted as a function of square root time. The resulting plots display pronounced regions of linearity between fractional uptakes of approximately 0.2 to 0.6. Assuming diffusion through a plane sheet of length l, this region is modeled with by the relationship:

$$\frac{q_t}{q_e} \propto \sqrt{\frac{D}{l^2} t} \qquad (8)$$

where D is the intracrystalline diffusivity.[23] Accordingly, the square of the slope in these plots corresponds to D/l^2, which is referred to as the diffusion time constant and has the units of inverse time. The temperature dependence of the diffusion time constant was then used to determine the activation energy to diffusion according to the Arrhenius expression:

$$\ln\frac{D}{l^2} = \frac{-E_a}{R}\frac{1}{T} + \ln A \qquad (9)$$

where E_a is the diffusion activation energy, R is the ideal gas constant, and A is the pre-exponential constant. The resulting plot of $ln(D/l^2)$ vs. $1/T$ is highly linear (see Figure 6c inset), and the obtained activation energy is -59(1) kJ/mol, where the error is defined as the standard error of the linear regression.

We note that the model used here technically assumes a constant pressure of adsorbate in the gas phase. Importantly, however, the dosed quantity was chosen such that changes in adsorbate pressure during the course of transient adsorption measurements are relatively small (approximately 15% between initial dosing and equilibration), which minimizes any errors arising from this assumption.

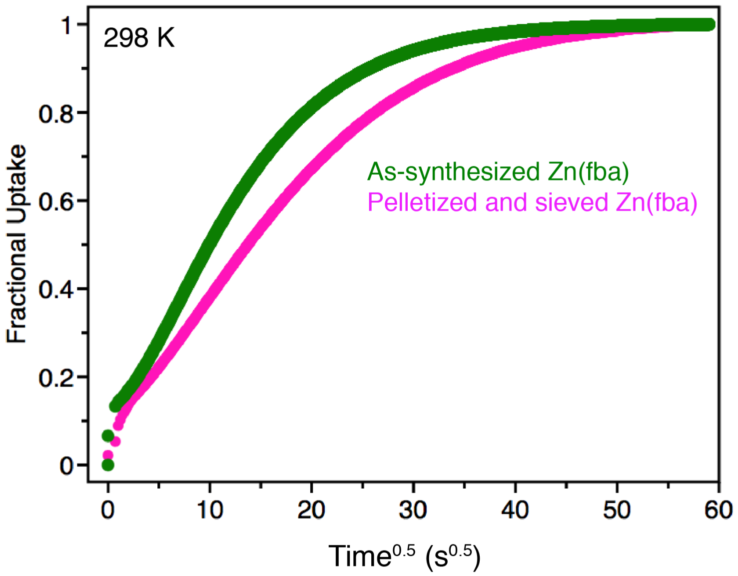

Figure S21. Comparative CF_4 transient adsorption data for Zn(fba) at 298 K using either as-synthesized material (green) or material that had been pelletized and then passed through mesh sieves to obtain a smaller dispersity of particle sizes (pink). The pelletized/sieved Zn(fba) samples were used for all subsequent transient adsorption measurements.

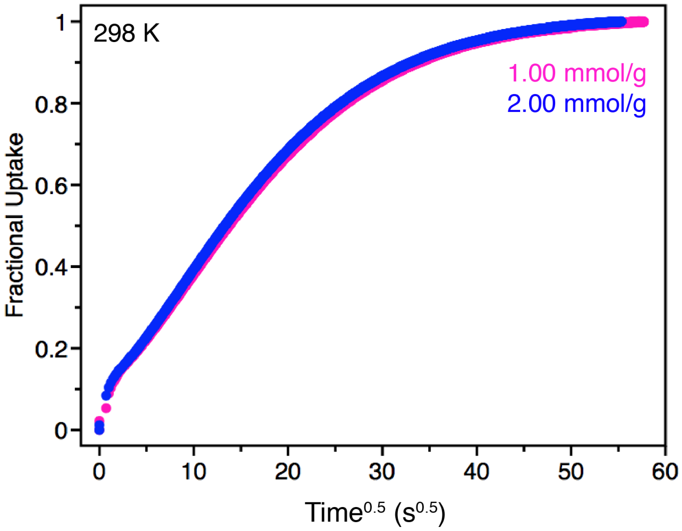

Figure S22. Tetrafluoromethane transient adsorption data for Zn(fba) at 298 K following either a 1.00 mmol/g (pink) or 2.00 mmol/g (dose) of adsorbate. This experiment was performed using 0.113 g of Zn(fba).

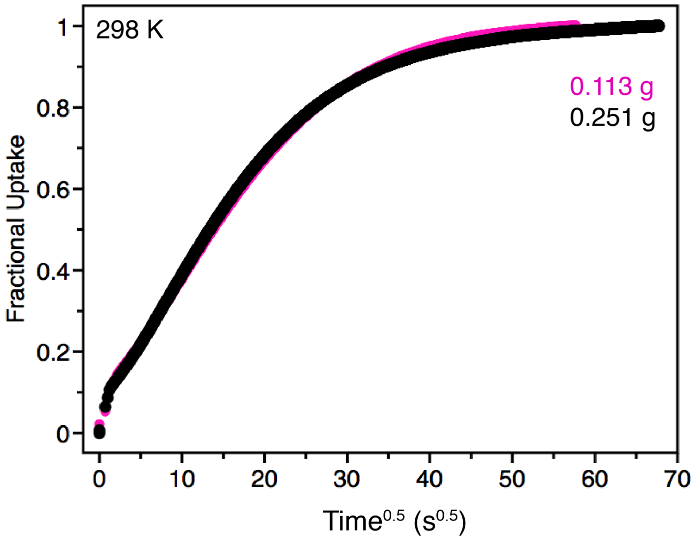

Figure S23. Tetrafluoromethane transient adsorption data for Zn(fba) at 298 K following a 1.00 mmol/g dose of adsorbate. These experiments were performed using either 0.113 g (pink) or 0.251 g (black) of Zn(fba).

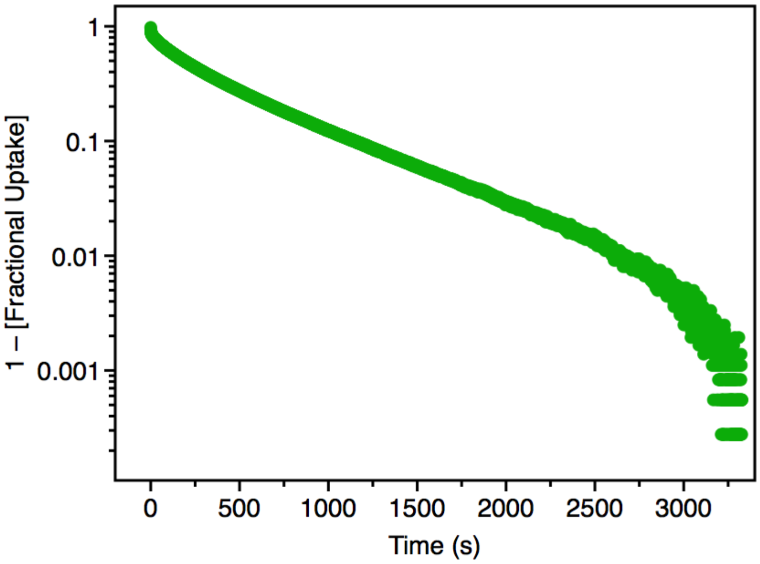

Figure S24. Semi-log plot of [1-(q_t/q_e)] vs. time for tetrafluoromethane transient adsorption into Zn(fba) at 298 K following a 1.00 mmol/g dose onto 0.113 g of MOF.

7. Column Breakthrough Measurements

Anhydrous Measurements. Breakthrough experiments were performed using a Micromeritics Autochem II 2920. Sieved sorbent samples were prepared by pressing the material into a pellet, and then passing it through two different mesh sieves with openings of 0.25 mm and 0.50 mm, respectively. The fraction that passed through the 0.50 mm sieve, but not through the 0.25 mm sieve, was collected and used for breakthrough measurements. The sorbent material was activated under 20 sccm of nitrogen by ramping to 90 °C at a rate of 1 °C/min and maintaining this temperature for one hour, then the temperature was increased to 250 °C at a rate of 5 °C/min and held for two hours. The sample was then cooled to room temperature, and at $t = 0$, the gas flow was switched to a pre-mixed cylinder comprised of 5:95 CF_4:N_2 at either 3 sccm or 20 sccm. Quantification of the CF_4 at the outlet was performed using a ThermoFisher Nicolet iS50 FTIR spectrometer by integrating the IR absorption peaks at wavenumbers between 1200 – 1300 cm^{-1}. A flowmeter at the outlet was used to monitor the time-resolved flow rate, which exhibited negligible variation across a given breakthrough experiment. The time-resolved concentration of N_2 at the outlet was determined by mass balance based on the time-resolved CF_4 concentration and outlet flow rate.

Investigating the Impact of Humidity on CF_4 Breakthrough Time. These measurements were performed using the setup depicted in Figure S30. Approximately 900 mg of Zn(fba) was placed and centered inside of the column, ensuring direct contact with the k-type thermocouple for controlled heating. For time-resolved analyte breakthrough and pre-exposure gas feed analysis a ThermoFisher Nicolet iS50 FTIR spectrometer and LiCor Li-850 were used. The feed stream was analyzed using the LiCor Li-850 prior to sample exposure for humidity measurements. To introduce water into the gas feed stream, a pre-mixed gas cylinder of 5% CF_4/N_2 was bubbled through MilQ water.

For each breakthrough run, the material was activated under a flow of 20 sccm of nitrogen by ramping sample temperatures to 90 °C at a rate of 1 °C/min and held at this sample temperature for one hour for gentle physisorbed water removal. The next step in the sample heating profile was to ramp to 250 °C at a rate of 5 °C/min, then hold for two hours at 250 °C. The sample was then cooled to 25 °C under the 20 sccm flowrate of nitrogen. Nitrogen was turned off once 25 °C was reached. The gas flow to the sample was then cut off using the intermediate ball valve. To introduce a controlled level of humidity into the analyte stream, the gas flow was set to 3 sccm and routed to the LiCor Li-850 analyzer to monitor water the composition as it equilibrated to about 2% of the feed stream on a molar basis. If the analyte gas conditions were dry, the gas was routed to avoid the bubbler and to Li-850 for 30 minutes. Once stable conditions were met for the feed stream, the analyte gases were then cut off from Li-850 route and fed into the sample column, where the effluent gas breakthrough times were monitored using the Nicolet iS50 FTIR spectrometer. 800mg of $CaSO_4$ desiccant was used in a dry tube placed in-line after the sample tube before reaching the MFC (used as flowmeter after the desiccant) and the FTIR spectrometer for equipment protection. CF_4 gas infrared (IR) interaction peaks (wavenumber 1200 – 1300 cm^{-1}) were integrated and plotted for 60 minutes under for "blank: control runs and 70 minutes run that involved the Zn(fba) sample. FTIR data acquisition always began two minutes before setting MFC to 3 sccm of feeds stream for vacant baseline observation.

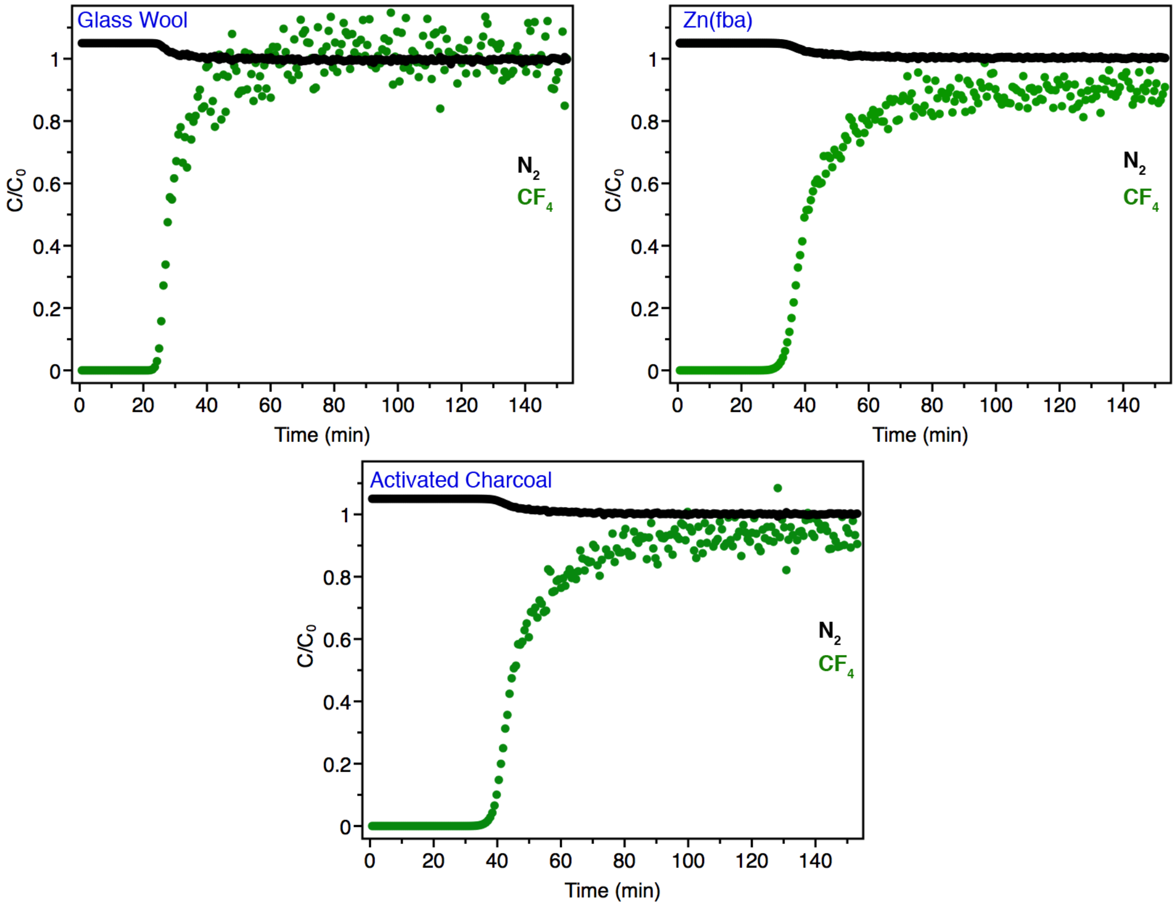

Figure S25. Column breakthrough measurements (5:95 CF_4:N_2) using a column packed with equivalent lengths of either glass wool, Zn(fba), or activated charcoal. The inlet flowrate was set to 3 sccm.

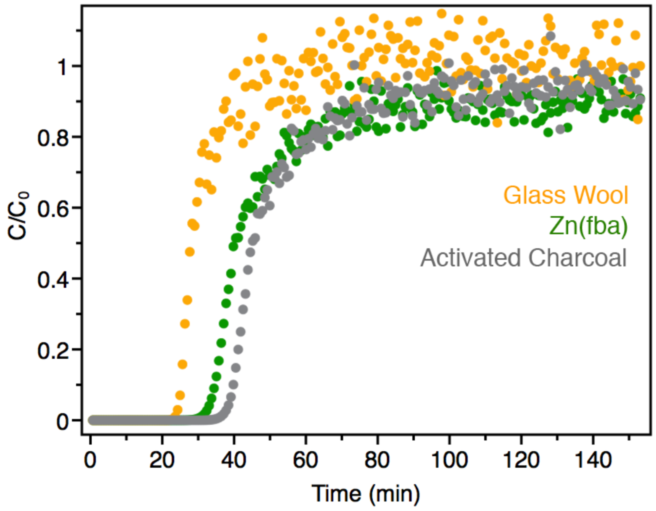

Figure S26. Comparative CF_4 breakthrough curves taken from the data depicted in Figure S25 (3 sccm flowrate).

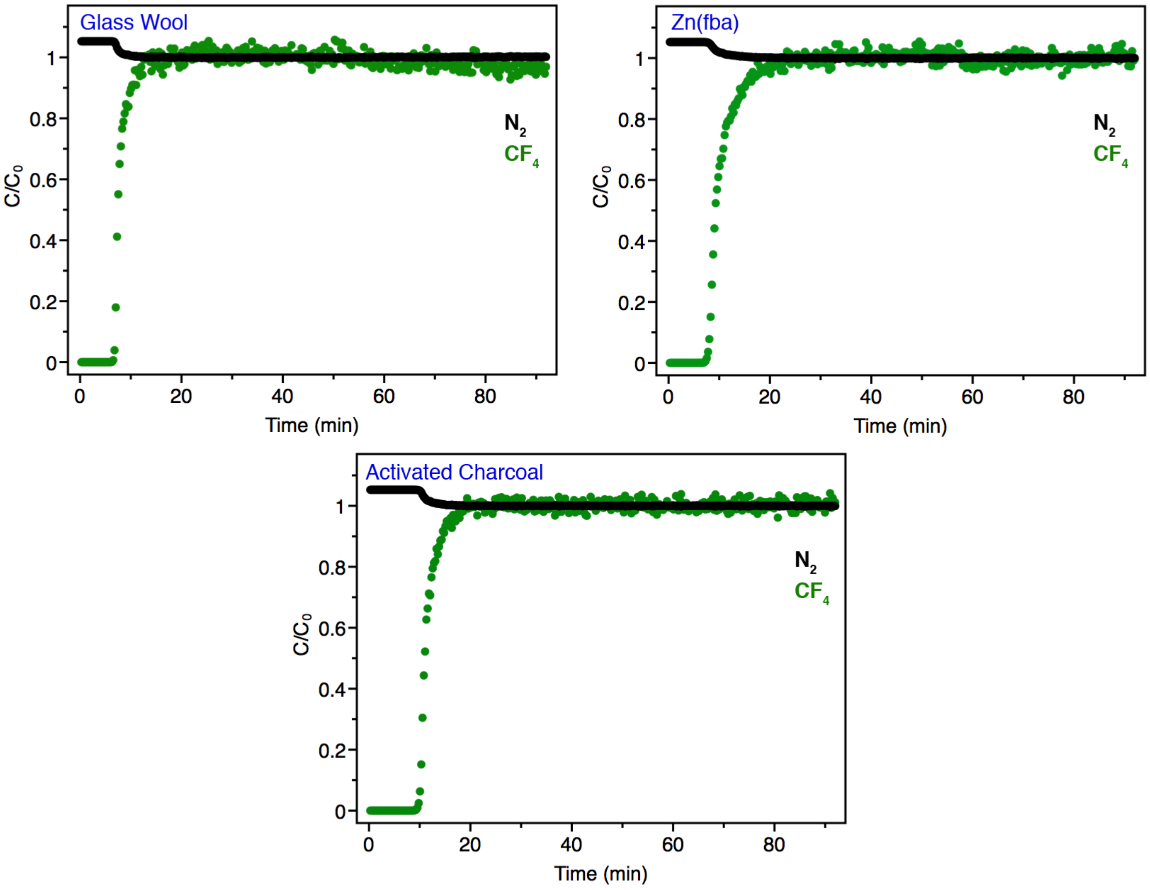

Figure S27. Column breakthrough measurements (5:95 CF_4:N_2) using a column packed with equivalent lengths of either glass wool, Zn(fba), or activated charcoal. The inlet flowrate was set to 20 sccm.

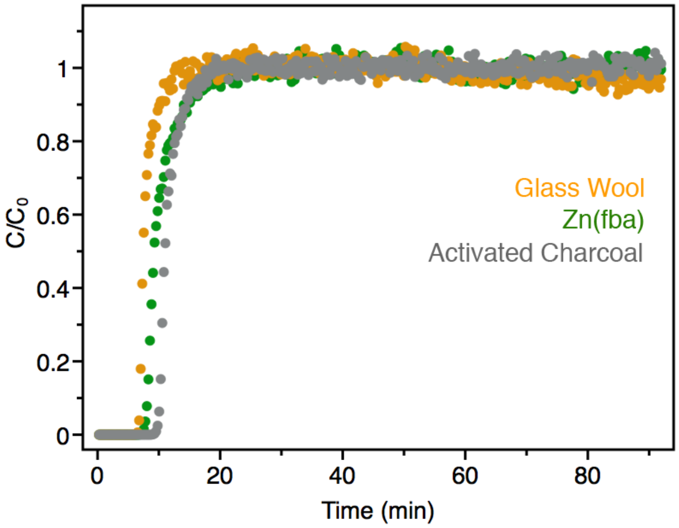

Figure S28. Comparative CF_4 breakthrough curves taken from the data depicted in Figure S27 (20 sccm flowrates).

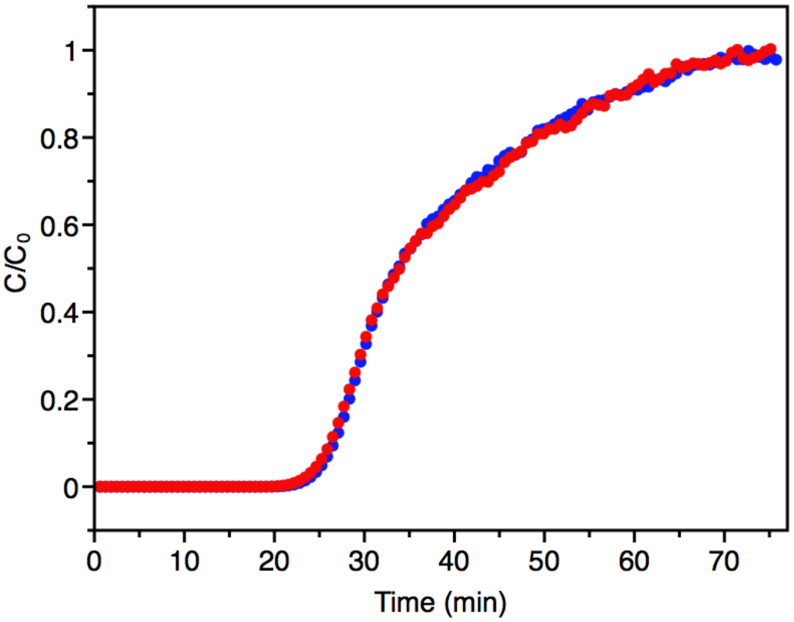

Figure S29. Comparative CF_4 breakthrough curves for Zn(fba) under humid (blue) and dry (red) conditions at 298 K and a total flow rate of 3 sccm.

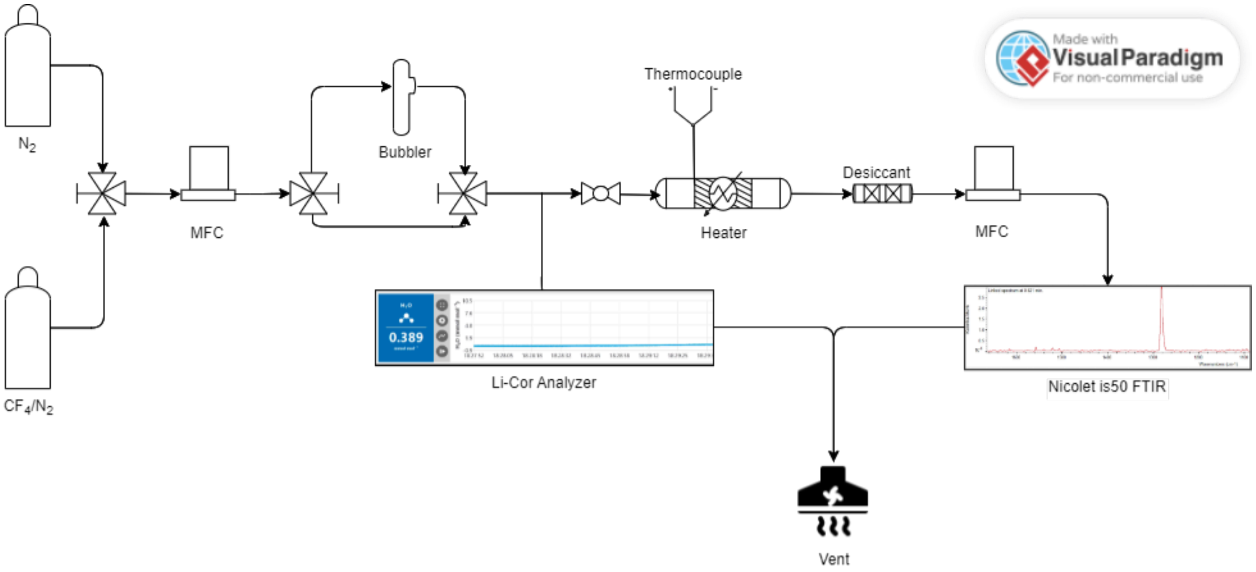

Figure S30. Schematic of the home-built apparatus used to study the effect of humidity on the CF_4 breakthrough performance of Zn(fba).

8. Scanning Electron Microscopy Measurements.

Scanning electron microscopy measurements were collected using a Zeiss Auriga Scanning Electron Microscope within the UR Nano Facility at the University of Rochester. The sample was dispersed in hexanes and transferred onto a silicon wafer which was mounted to an Al SEM stub using carbon tape. The sample was imaged at a working distance of 2.9 mm and an accelerating voltage of 0.5 kV using an in-lens secondary electron detector.

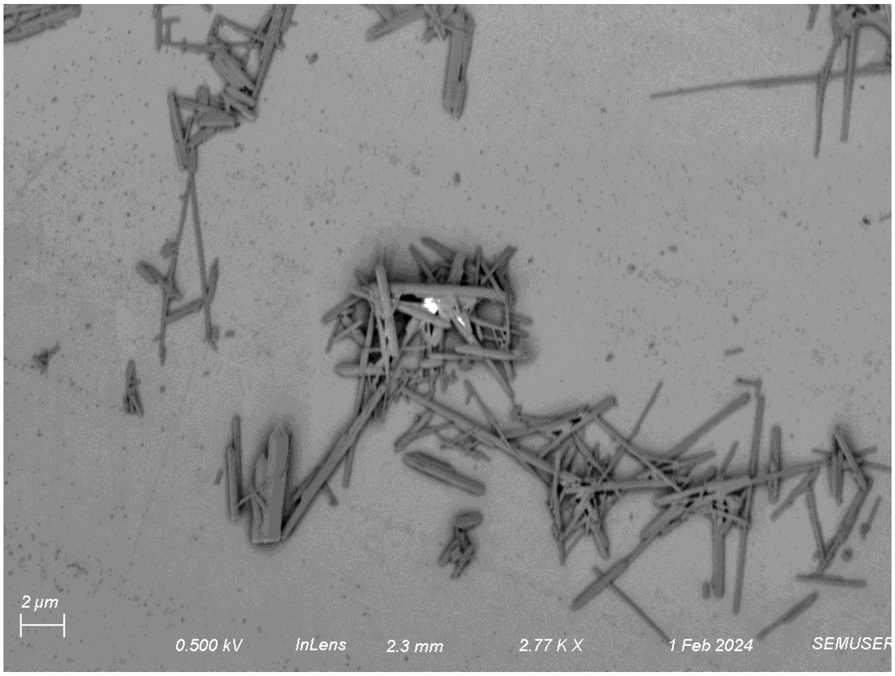

Figure S31. SEM image of a sample of Zn(fba) that has not been pelletized and sieved.

9. References

1. Monge, N. Snejko, E. Gutiérrez-Puebla, M. Medina, C. Cascales, C. Ruiz-Valero, M. Iglesias and B. Gómez-Lor, *Chem. Commun.*, 2005, 1291–1293
2. S.M. Wang, H.-L. Lan, G.-W. Guan and Q.-Y. Yang, *ACS Appl. Mater. Interfaces*, 2022, **14**, 40072–40081.
3. A. L. Myers and J. M. Prausnitz, *AIChE J.*, 1965, **11**, 121–127.
4. Y. Wu, T. Yan, W. Zhang, S. Chen, Y. Fu, Z. Zhang and H. Ma, *Ind. Eng. Chem. Res.*, 2022, **61**, 13603–13611.
5. Z. Wan, T. Yan, M. Chang, M. Yang and D. Liu, *Separation Purification Technol.*, 2023, **306**, 122617.
6. X. Huang, F. Chen, H. Sun, W. Xia, Z. Zhang, Q. Yang, Y. Yang, Q. Ren and Z. Bao, *Separation Purification Technol*, 2022, **292**, 121059.
7. P. Gao, Z. Wang, L. Liu, S. Cheng and G. Li, *J. Taiwan Inst. Chem. Eng.* 2023, **143**, 104654.
8. J. Zhu, J. Hu, H. Xiao, L. Yang, M. Yang, S. Wang, J. Zhang and H. Xing, *Separation Purification Technol*, 2024, **331**, 125614.
9. J. Wang, W. Fu, L. Wang, Y. Li, Y. Li, Z. Sui and X. Xu, *Chem. Eng. J.*, 2023, **477**, 147128.
10. X. Yuan, M.-K. Cho, J. G. Lee, S. W. Choi and K. B. Lee, *Environ. Pollution*, 2020, **265**, 114868.
11. X. Yuan, S. W. Choi, E. Jang and K. B. Lee, *Chem. Eng. J.*, 2018, **336**, 297–305.
12. S. W. Choi, D.-H. Lee, J. Kim, J. Kim, J.-H. Park, H. T. Beum, D.-S. Lim and K. B. Lee, *Chem. Eng. J.,* 2017, **311**, 227–235.
13. S. W. Choi, H. J. Yoon, H. J. Lee, E.-S. Lee, D.-S. Lim and K. B. Lee, *Microporous Mesoporous Mater.*, 2020, **306**, 110373.
14. Y. Wu, S. Wang, W. Zhang, S. Chen, Z. Zhang, B. Yang, S. Li and H. Ma, *Separation Purification Technol* 2022, **289**, 120739.
15. W. Zhang, Y. Wu, Y. Li, S. Chen, Y. Fu, Z. Zhang, T. Yan, S. Wang and H. Ma, *Macromolecules*, 2022, **55**, 1435–1444.
16. W. Zhang, Y. Li, Y. Wu, Y. Fu, S. Chen, Z. Zhang, S. He, T. Yan and H. Ma, *Separation Purification Technol*, 2022, **287**, 120561.
17. N.-G. Ahn, S.-W. Kang, B.-H. Min and S.-S. Suh, *J. Chem. Eng. Data*, 2006, **51**, 451–456.
18. S. W. Choi, S.-M. Hong, J.-H. Park, H. T. Beum and K. B. Lee, *Ind. Eng. Chem. Res.*, **54**, 8561–8568.
19. CrysAlisPro, version 171.42.90a; Rigaku Corporation: Oxford, UK, 2023.
20. Sheldrick, G. M. SHELXT, version 2018/2; Acta. Crystallogr. 2015, A71, 3-8.
21. Sheldrick, G. M. SHELXL, version 2019/3; Acta. Crystallogr. 2015, C71, 3-8
22. Dolomanov, O. V.; Bourhis, L. J.; Gildea, R. J.; Howard, J. A. K.; Puschmann, H. Olex2, version 1.5; J. Appl. Cryst. 2009, **42**, 339-341.
23. J. Crank, *The Mathematics of Diffusion*, Clarendon Press, Oxford, 2nd ed., 1975.